Quantifying Plio-Pleistocene global mean sea-level variation

FD Richards, Department of Earth Science & Engineering, Imperial College London, South Kensington, London, United Kingdom

Abstract

Future sea-level rise poses an imminent threat to coastal communities, and actionable sea-level forecasts are urgently needed to ensure they are adequately protected. Such projections cannot be developed without deep understanding of the mechanisms driving sea-level change and how they responded in the past to climatic forcings akin to those expected in the near future. Quantifying the amplitudes of Plio-Pleistocene sea-level highstands, and their correlation with other palaeoclimatic variables, is therefore of critical societal importance. Here, I review the geodynamic processes that complicate sea-level reconstructions and how associated ice volume estimates have evolved with improved understanding of these phenomena.

Keywords

Dynamic topography; Geoid; Glacial isostatic adjustment; Last interglacial; Mid-Pliocene warm period; Palaeoclimate; Sea level

Key points

- Global mean sea level (GMSL) during past warm periods can only be determined from geomorphic records after careful correction for relative sea-level (RSL) changes caused by solid Earth processes.
- RSL variations caused by dynamic topography and glacial isostatic adjustment (GIA) are ubiquitous and are often of comparable magnitude to GMSL variations, making them especially important to constrain.
- Recent observational, theoretical, and computational advances allow these processes to be modeled with far greater accuracy, improving accuracy and uncertainty quantification of Plio-Pleistocene GMSL estimates.
- Revised understanding of past GMSL can significantly reduce the considerable uncertainties that currently exist in ice-sheet-model-based sea-level projections.

Introduction

Deepening our understanding of the long-term relationship between sea-level and climate forcing is key to developing more accurate and actionable projections of future sea-level change. While instrumental records yield direct and precise measurements of Earth's modern climatic evolution, they are generally brief (<60 years) and may be of limited relevance to the more extreme environments that could prevail in the near future, restricting their usefulness for inferring future trends. Geological proxy records,

although indirect and less complete, provide complementary constraints on sea level and climate covariation over a broader range of conditions, helping to refine sea-level forecasts on decadal to centennial timescales. Measurements from the most recent periods of enhanced warmth and high *global mean sea level* (GMSL) are especially valuable since these intervals represent the closest analogues to near-future climate states. Considerable focus has therefore been placed on reconstructing sea level and ice sheet configuration during the Mid-Pliocene Warm Period (MPWP; ~3.3–3.0 Ma) and the Last Interglacial (LIG; ~129–116 ka), periods characterized by global mean temperatures ~2°C–3°C and ~1°C above preindustrial values, respectively.

GMSL variations since the onset of the Pliocene period, ~5.3 million years ago, have generally been inferred using either temperature-corrected oxygen isotope compositions of foraminifera and ostracods (often in conjunction with Mg/Ca ratios; Raymo et al., 2018), or elevations of geomorphic sea-level indicators, such as palaeoshoreline deposits and backstripped sedimentary successions (Miller et al., 2020). The former approach provides a continuous record of GMSL variation across the past few million years, but is subject to considerable uncertainty due to analytical precision limitations, difficulties discriminating between temperature and ice volume signals, and poorly constrained diagenetic effects. These geochemically derived GMSL estimates are therefore accurate to no better than ~±15 m (Raymo et al., 2018). Since these uncertainties are comparable to the differences between present-day sea level and peak sea level during past warm periods, efforts to quantify past highstand amplitudes have generally focused on palaeoshoreline records. While these geomorphic proxies can potentially provide more accurate GMSL constraints, care must be taken to account for processes that cause locally recorded *relative sea level* (RSL) changes to deviate from globally averaged signals.

Here, I describe these physical mechanisms and review the characteristic magnitudes and timescales of the RSL variations they produce. Next, advances in modeling and removing their effects are discussed, as well as the impact these breakthroughs have had on our current understanding of major Pliocene–Recent highstands. Finally, outstanding challenges are summarized, with suggestions offered for how best to leverage new datasets and modeling techniques to make progress in these areas.

Physical drivers of Pliocene-to-Recent relative sea-level change

Geomorphic proxies record changes in RSL, which is equivalent to the elevation difference between the solid Earth and the ocean surface. Processes that vertically perturb either boundary can therefore cause RSL to deviate from GMSL (the area-weighted mean of RSL), and these displacements must be accurately quantified before sea-level markers can be used to infer ice volumes. Over short timescales (10^{-2}–10^{1} years), local RSL variations of up to a meter can be caused by ocean dynamics ('dynamic ocean topography'), subsidence due to groundwater depletion, and major earthquakes. However, on the longer timescales (10^{4}–10^{6} years) relevant to Plio-Pleistocene warm periods, several additional mechanisms start to dominate the RSL signal: glacial isostatic adjustment (GIA; i.e., sea-level and topography variations caused by ice and ocean mass changes); mantle dynamic topography (i.e., vertical deflections of Earth's solid surface driven by mantle convection); sustained tectonic activity; erosion and sedimentation (including carbonate dissolution and precipitation); and magmatic processes (e.g., underplating and volcanic loading).

Glacial isostatic adjustment

At periodic intervals over the past ~3 million years, Earth's polar ice sheets have expanded far beyond their present footprint during *glacials*, particularly in the Northern Hemisphere where large fractions of the North American and Eurasian continents have been covered by kilometer-thick ice masses, termed the Laurentide and Fennoscandian ice sheets, respectively (Raymo, 1994). These glacials have been punctuated by *interglacial* periods, in which ice sheets rapidly collapsed back to a configuration similar to their present extent. During these glacial–interglacial cycles, exchange of water between ice and ocean reservoirs has been sufficient to raise and lower GMSL by ~100 m. These huge mass transfers trigger deflections of both the Earth's solid surface and its *geoid* (the gravitationally controlled equilibrium shape of the ocean surface) that are collectively referred to as GIA.

Since the solid Earth deforms like a viscoelastic material, the GIA signal associated with the growth and decay of ice sheets comprises both an elastic component, which responds instantaneously to changing ocean and ice loads, and a viscous component, which exhibits time-dependent behavior. The latter contribution, coupled with high mantle viscosities, explains why the crust is still rebounding in areas previously covered by the Laurentide and Fennoscandian ice sheets despite their collapse ending over 7 thousand years ago. This *postglacial rebound* or *glacioisostasy* is manifest in the ongoing sea-level fall of ~10 mm year^{-1} in parts of Hudson Bay and the Gulf of Bothnia (Fig. 1A; Bungum and Eldholm, 2022). Similarly, faster-than-average sea-level rise in regions such as Chesapeake Bay results from subsidence of the peripheral bulge surrounding the former ice sheets.

Glacioisostatic surface deflections dominate the signal of GIA-induced RSL change in *near-field* regions close to ice sheet margins. However, in *far-field* locations remote from ice sheets, geoid and surface perturbations associated with shifting ocean loads, collectively referred to as *hydroisostasy*, are most prominent. One key hydroisostatic mechanism is *continental levering*, whereby water loading of previously air-loaded margins during deglaciation induces ~0.5 mm year^{-1} subsidence offshore and up to ~1 mm year^{-1} uplift onshore (Fig. 1B; Mitrovica and Milne, 2002). The increase in ocean basin volume that ensues, combined with that caused by peripheral bulge collapse in the near field, draws water away from equatorial regions, resulting in ~0.5 mm year^{-1} sea-level fall at low-latitude ocean islands in a second hydroisostatic process known as *equatorial ocean siphoning* (Fig. 1C).

Variations in glacial loading also perturb Earth's inertia tensor, modifying the orientation of the solid Earth with respect to its spin axis. The shift in the position of the equatorial bulge caused by this *true polar wander* creates a long-wavelength (~15,000 km)

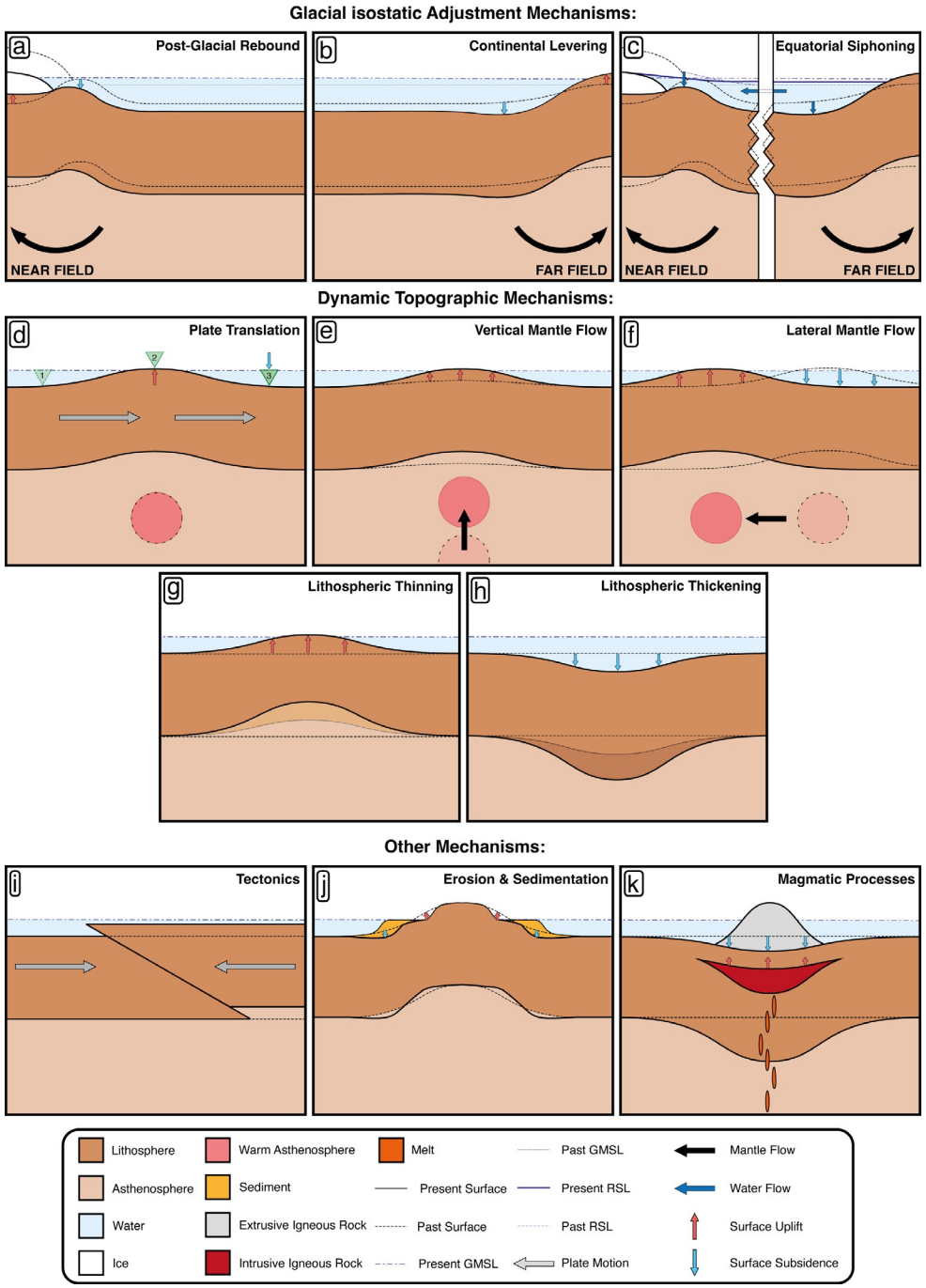

Fig. 1 Processes affecting long-term RSL change. (A) Postglacial rebound. Surface uplift beneath ice sheet following melting; subsidence in peripheral bulge region. (B) Continental levering. Surface uplift along continental margin following ice sheet melting; subsidence offshore. (C) Equatorial ocean siphoning. Water migration to subsiding regions following ice sheet melting (i.e., peripheral bulge and offshore continental margins) causes far-field RSL fall; reduced gravitational pull of ice sheet drives near-field RSL fall. (D) Plate translation. *Green arrows* mark locus of sea-level marker as a function of time. (E) Vertical mantle flow. (F) Lateral mantle flow. (G) Lithospheric thinning. (H) Lithospheric thickening. (I) Tectonics, including short-term pre-/co-/post-seismic deformation and long-term crustal thickening/thinning. (J) Erosion and sedimentation, including carbonate dissolution/precipitation. (K) Magmatic processes, including surface subsidence from volcanic loading/uplift from magmatic underplating.

pattern of relative uplift in regions that move closer to the new equator and subsidence elsewhere. This mechanism is responsible for the progressive shift of Earth's rotation axis toward Hudson Bay since the Last Glacial Maximum (LGM; 27 ka). Although the impact of this rotational feedback on RSL is relatively small (10^1–10^2 times less than that due to glacioisostasy), it is a non-negligible contributor to far-field patterns (Mitrovica et al., 2005).

The GIA-induced RSL changes described above mostly result from the displacement of Earth's solid surface. However, the evolution of Earth's gravitational field during glacial cycles also significantly alters spatial patterns of RSL change through both the instantaneous *direct effect* of ice-sheet-to-ocean mass flux and the slower-evolving *indirect effect* arising from solid Earth responses to this mass transfer. For example, the direct effect of melting the Greenland Ice Sheet would manifest in a nearly instantaneous sea-level fall in Scotland and other near-field sites (e.g., Northern Labrador) because ocean surface lowering caused by the ice sheet's reduced gravitational pull would locally overwhelm the effect of adding water to the global ocean (Kopp et al., 2015). By contrast, the indirect effect of this melting would be apparent in local increases in the ocean surface height resulting from mass flux of solid Earth material into the region previously depressed by the former ice load.

Note that, in addition to affecting patterns of RSL change, GIA impacts the relationship between palaeo-ice volume and GMSL by altering the geometry of ocean basins. For example, it is estimated that complete collapse of the Greenland and West Antarctic ice sheets would drive sufficient surface rebound in these regions to eventually (after $\sim 10^4$ years) reduce ocean basin volume by an amount equivalent to 2 m of GMSL. The total increase in GMSL resulting from this ice-to-water mass transfer would therefore be 14 m rather than the 12 m expected if a fixed, present-day ocean basin geometry were assumed (Raymo et al., 2011).

During post-Pliocene ice age cycles GIA processes have acted in concert to generate $\sim 10^0$–10^2 m deviations in local sea-level from contemporary GMSL (Horton et al., 2018). Although this signal is more muted in regions remote from the evolving land-based ice masses, its ubiquity means that, even at far-field sites, geomorphic palaeo-sea-level records must be carefully corrected when estimating palaeo-GMSL and ice volume (Fig. 2). An added complication is that, while viscosity might locally be low enough to produce centennial or decadal relaxation times, on a global scale, relaxation times are typically multimillennial (Barletta et al., 2018). This long timescale means that the solid Earth system has never fully reached isostatic equilibrium during any post-Pliocene glacial cycle. Recovery from preceding ice and ocean load changes has therefore been continuously interrupted and overprinted by the onset of the next cycle. These complexities make detailed knowledge of mantle viscosity and ice sheet history a prerequisite for determining palaeo-GMSL variations from geomorphic RSL markers.

Mantle dynamic topography

Although most of Earth's topography is *isostatic* (i.e., controlled by variations in the thickness and density of the crust and lithosphere), stresses exerted on the base of the lithosphere by convective flow within the underlying mantle can also generate km-scale topographic variations (Hoggard et al., 2021). This so-called mantle *dynamic topography* is ubiquitous and continuously evolves along with the planform of convection, causing vertical deflections of Earth's solid surface that vary substantially as a function of space and time. These mantle-driven vertical motions were originally thought to evolve slowly (< 5 m Myr^{-1}; e.g., Müller et al., 2008) and therefore to have negligible impact on LIG ($\sim$129–116 ka) palaeoshoreline elevations and limited influence on MPWP ($\sim$3.3–3.0 Ma) counterparts. However, recent studies have inferred rates of ~ 100 m Myr^{-1}, suggesting that dynamic topography is an important consideration for palaeoshoreline-based inferences of GMSL during all warm periods pre-dating the Holocene (Fig. 2; Hoggard et al., 2021).

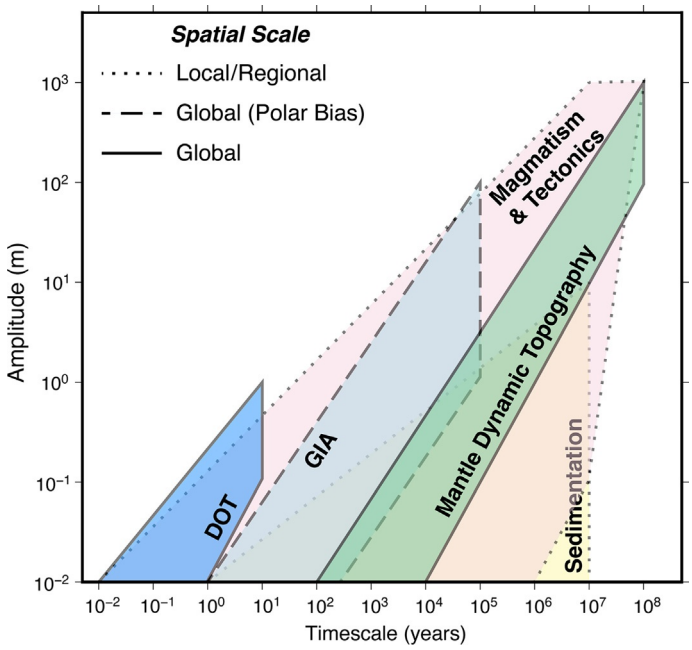

Fig. 2 Characteristic duration and magnitude of processes affecting RSL variation. DOT = Dynamic ocean topography. Note that although magmatism, tectonics, and sedimentation can generate >10 m RSL change on long timescales, their influence is localized.

Spatio-temporal changes in dynamic topography can be generated via a range of end-member mechanisms including plate translation over a fixed convective planform (Fig. 1D), vertical and lateral convective flow of internal density anomalies (Fig. 1E and F), and changes in lithospheric thickness (Fig. 1G and H). Several of these processes may be acting simultaneously in a given geodynamic context. For example, upwelling of hot mantle material will often drive lithospheric reheating and thinning, with the total reduction in lithospheric thickness potentially depending on the rate of plate translation over this convective planform. Consequently, it is often difficult to accurately quantify these different contributions to overall dynamic topography change.

In addition to inducing spatially variable RSL changes, dynamic topography may affect GMSL directly, for example, by generating net uplift over ocean basins (e.g., $\sim$ 1 m Myr^{-1} Conrad and Husson, 2009), or by altering equilibrium ice sheet thickness through deflection of subglacial topography. For example, an additional contribution to MPWP sea level of 1–3 m has been attributed to relative depression of Wilkes Basin topography during this period (Austermann et al., 2015).

Tectonics

Steady accumulation of fault-related vertical land motions can cause significant RSL change over the timescales relevant to Plio-Pleistocene GMSL reconstruction (Fig. 1I). The rate of this tectonic uplift and subsidence varies widely from location to location, with stable cratonic regions (e.g., western Australia, Scandinavia, and central North America) inferred to have experienced negligible tectonic activity ($\leq$0.01 mm year^{-1}; e.g., Burbidge et al., 2009) while convergent plate margins record rates of 1–10 mm year^{-1} (e.g., Papua New Guinea, and the Alaskan and British Columbian stretches of the Pacific Coast Ranges; Pfeffer et al., 2017; Fig. 2). Correcting for these perturbations is complicated by the fact that many long-term uplift and subsidence estimates are derived from thermochronological data with low spatio-temporal resolution, potentially aliasing short-timescale tectonic RSL changes at certain sites. Nevertheless, high uplift rates can promote the formation and preservation of flights of marine terraces from multiple sea-level highstands. Vertical separation between these terraces may therefore allow relative GMSL variation within individual glacial cycles to be deduced, provided uplift rates can be independently constrained and assumed to be relatively constant on these 10^4-year timescales (Malatesta et al., 2022).

On long timescales, rifting of passive margins, continental collision, and changes in mid-ocean ridge spreading rate can drive significant GMSL variation by modifying the total volume of ocean basins (Wright et al., 2020). There is some controversy regarding the true magnitude of these GMSL variations. For example, it has been argued that age-dependent subsidence of the cooling oceanic lithosphere should be included in the definition of dynamic topography (Forte and Rowley, 2022). In this formalism, changes in spreading rate and the average age of oceanic lithosphere would constitute a shift in oceanic mantle dynamic topography that must be compensated by an opposing shift in continental regions since the global integral of this field should be equal to zero. If confirmed, this compensation mechanism would imply that many long-term sea-level estimates are inaccurate because they assume that continental hypsometry is time-invariant. However, a recent numerical modeling study that simultaneously accounts for changes in oceanic and continental topography finds that increased mid-ocean ridge spreading rate tends to correlate with more elevated continental dynamic topography, the opposite trend to that expected if such compensation were in operation (Young et al., 2022). Clearly, further work is needed to clarify this matter, but whatever the outcome of the debate, the total amplitude of tectonic GMSL change is not thought to have exceeded $\sim$1 m Myr^{-1} in the past 5 Myrs, although revised plate reconstructions do suggest a global slowdown in spreading rate that may have generated more pronounced GMSL reduction between 15 and 5 Ma (Dalton et al., 2022).

Erosion and sedimentation

Transfer of rock mass via erosion and sedimentation, or precipitation and dissolution, alters the position and amplitude of surface loads applied to the crust. This shift in loading pattern perturbs both the geoid and Earth's solid surface and can therefore lead to significant RSL change ($\sim$0.05–0.5 mm year^{-1}) in mountainous areas and coastal regions that are subject to karstification, or close to major sedimentary depocenters (e.g., deltas and coral reefs; Creveling et al., 2019; Pico, 2020; Fig. 1J). In addition, unconsolidated sediment will compact under its own weight, expelling water from its pore space into the global ocean and potentially lowering solid surface elevations by up to 5 mm year^{-1} along coastal plains and deltas (Fig. 2). Observational constraints on past sediment flux are therefore essential for inferring palaeo-GMSL from RSL markers deposited on top of poorly consolidated sediment or at sites proximal to major deltas or reefs. The viscoelastic properties of the lithosphere around these depocenters must also be estimated since they control the amplitude and wavelength of sedimentation-related uplift and subsidence (Watts, 2001).

GMSL can also be affected by sedimentation patterns. For example, increased sediment deposition and carbonate precipitation will displace water, leading to sea-level rise. Although such variations in the global sediment budget are partially compensated by loading-induced crustal deflections, they can have a non-negligible impact on long-term GMSL trends ($\sim$0.5 m Myr^{-1}; Young et al., 2022).

Magmatic processes

The impact of magmatic processes on long-term RSL changes is most apparent at ocean islands. Progressive growth of their volcanic edifices load the crust, driving subsidence of fringing RSL markers at rates of up to $\sim$5 mm year^{-1} (Huppert et al., 2015; Fig. 1K). At the same time, crustal thickening via underplating of intrusive material close to the crust-mantle boundary can drive countervailing

isostatic uplift of ocean islands, albeit at slower rates (~0.05 mm year^{-1}; Ramalho et al., 2017; Fig. 2). An additional consideration when assessing magmatic impacts is that even after volcanic activity has ceased on one island, RSL indicators can be perturbed by the ongoing growth of adjacent loads, as is commonly the case in ocean island chains created by plate motion over a relatively stationary mantle plume (Huppert et al., 2015). These substantial changes in land elevation inevitably complicate efforts to constrain GMSL on ocean islands that are either volcanically active, or else located close to sites of active magmatism.

Changes in the rate of magmatic addition to the crust and lithosphere also affect ocean basin volume, modulating GMSL on long timescales. In particular, eruptions of submarine *Large Igneous Provinces* (e.g., the Ontong-Java Plateau) can potentially cause punctuated meter-scale increases in GMSL. Nevertheless, despite a significant contribution to the sea-level budget (~20–50 m GMSL equivalent; GMSLE; Wright et al., 2020; Young et al., 2021), available evidence suggests that, on 10^0–10^1 Myr timescales, submarine eruption rates and their impact on sea-level have varied minimally since 200 Ma (~0.1 m Myr^{-1}).

Quantifying GMSL variations from geomorphic proxies

Geomorphic records of palaeo-sea-level variation are invariably affected by some combination of the post-depositional processes detailed above. Inferring GMSL variation from these observations therefore requires analysis to be restricted to regions where each of these perturbations can either be accurately quantified, or else assumed to have negligible impact. Unfortunately, no site on Earth preserves a pristine record of palaeo-sea-level change since two of these processes—GIA and dynamic topography—are ubiquitous and must therefore be constrained. At sites remote from major ice sheets, incomplete knowledge of mantle rheology and past ice configuration translates into relatively minor uncertainty in GIA-induced RSL change, allowing useful inferences of palaeo-GMSL to be drawn. However, the impact of uncertain mantle structure on dynamic topography is of comparable magnitude everywhere on Earth's surface and must be accounted for at all localities when inferring pre-Holocene sea level.

The relationship between different sea-level proxies (e.g., salt marsh sediments, fossil reefs, beach deposits, marine terraces, and archaeological records) and time-integrated mean sea level, also known as the *indicative range* of a sea-level indicator, introduces further uncertainty into GMSL inferences. For example, the elevation above mean sea level of a beach ridge strongly depends on local wave energy (1–6 m) while corals often have wide habitat depth distributions (~−10–0 m) that vary by species (Hibbert et al., 2016). The precision to which these different markers can be dated varies according to the analytical technique used, which depends in turn upon their composition, preservation, and overall age (e.g., radiocarbon dating is typically more precise than U-Th dating, but is only feasible for sea-level indicators less than ~50,000 years old; Murray-Wallace and Woodroffe, 2014). Age uncertainties can therefore become large compared with the length of a target interglacial or warm period, especially for older sea-level indicators.

Despite these uncertainties associated with geodynamic processes, palaeo-water depth, and age of formation, geomorphic sea-level indicators can generally constrain interglacial GMSL better than isotopic records. The MPWP and LIG have been of particular interest since climate during these periods was sufficiently similar to that of the present day and expected near future that studying their sea-level histories may help to predict changes over the coming centuries. Our understanding of sea level during these periods is therefore the focus of the following section; however, other key Plio-Pleistocene warm periods are summarized to add context.

Mid-Pliocene Warm Period

The MPWP, 3.0–3.3 million years ago, represents the most recent time in Earth history that atmospheric CO_2 concentrations and global mean temperatures reached values approaching those expected over the course of the next century (~340–460 ppm and ~2°C–3°C above pre industrial; Rae et al., 2021). Consequently, estimates of GMSL during this period are valuable for ongoing efforts to determine future ice sheet stability in the face of prolonged warming.

Determining MPWP palaeo-ice volume from geomorphic proxies is complicated by the potential for convectively driven $\sim10^1$–10^2 m surface deflections to have accrued over the 3 million years that have elapsed since this time interval. Although inferences of palaeo-ice volume from isotopic datasets partly circumvent this issue, MPWP GMSL estimates derived in this way range from 6 to 58 m above present day values (Grant and Naish, 2021). Provided post-depositional effects can be reliably constrained and corrected for, geomorphic proxies are therefore more likely to yield accurate and precise GMSL constraints. Indeed, the range of published values derived from geomorphic data is narrower than the geochemically inferred equivalent (+6–35 m versus +6–58 m) despite including estimates that make no attempt to correct for dynamic topography.

The amplitude of glacial-to-interglacial GMSL change during the MPWP can be determined relatively reliably at far-field sites because slow-evolving dynamic topographic perturbations can be separated from the shorter period ($\sim10^4$-year) glacioeustatic cycles. For example, high-resolution sedimentary records from the Whanganui Basin in New Zealand indicate a difference in GMSL between MPWP glacials and interglacials of between 6 and 17 m (16th and 84th percentiles; Grant and Naish, 2021). However, such records are unable to constrain absolute values of MPWP GMSL compared to the present-day without independent knowledge of ice sheet configuration during at least one of these mid-Pliocene intervals.

Absolute GMSL can be obtained in locations where a sufficiently long and continuous record of RSL change is available. In such cases, mantle-driven uplift or subsidence can be estimated by comparing the vertical separation between sea-level markers formed during different warm periods to expected relative GMSL differences derived from independent reconstructions. This approach has been applied to 3.1–4.8 Ma RSL variations recorded by phreatic overgrowths in Mallorcan caves, yielding long-term uplift rates of 0.6–4.4 m Myr^{-1} and corrected MPWP GMSL of +6.8–20.4 m (including a +1.2 m thermosteric contribution; Dumitru et al., 2019).

An alternative strategy, made possible by recent improvements in our understanding of Earth's three-dimensional density and viscosity structure, is to constrain dynamic topography directly using simulations of mantle convection. For example, an MPWP GMSL of ~15 m has been inferred by correcting the elevation of the ~800 km-long Orangeburg Scarp palaeoshoreline (Eastern USA) for predicted post-depositional deflections due to dynamic topography, as well as GIA and flexural deformation arising from erosion and sedimentation (Moucha and Ruetenik, 2017). However, the limited range of convection simulations typically applied in such studies, and their restriction to single localities, makes it difficult to quantify the impact of uncertain mantle structure and evolution on the final GMSL estimate. Moreover, in the specific case of the Orangeburg Scarp, GIA and sediment loading are also important factors due to its proximity to the former Laurentide Ice Sheet and substantial post-Pliocene sediment deposition offshore, each translating into potentially significant but poorly quantified GMSL uncertainties.

Many of these limitations can now be addressed through methodological refinements. First, *emulators* (i.e., computationally efficient approximators) can be trained on ensembles of mantle convection and GIA simulations that provide acceptable fit to geodynamic observables. Once appropriately calibrated, these emulators can rapidly calculate post-depositional deflections for a broad range of uncertain Earth model parameters. By integrating these functions into a probabilistic inverse framework, it is then possible to robustly propagate uncertainties in solid Earth structure into MPWP GMSL estimates. Second, by simultaneously correcting geomorphic RSL data from multiple sites, a more globally representative GMSL value can be obtained, while also improving constraint on Earth's internal structure based on which density and viscosity inputs best reconcile the vertical offset between sea-level markers at different sites. Finally, by concentrating on regions remote from major ice sheets with minimal tectonic activity and slow rates of erosion and sedimentation, uncertainty associated with post-depositional processes can be minimized, increasing the precision of GMSL estimates. A recent application of this approach to a suite of continent-wide offshore and onshore RSL constraints around Australia yields an MPWP sea-level estimate of $+16.0^{+5.5}_{-5.6}$ m (Richards et al., 2022; Fig. 3).

Although efforts to correct MPWP sea-level markers for dynamic topographic perturbations remain at an early stage, estimates that do correct for this long-term uplift and subsidence suggest that GMSL was at least 7 m above present, but reached no higher than +21 m (Moucha and Ruetenik, 2017; Dumitru et al., 2019; Hearty et al., 2020; Richards et al., 2022). After accounting for an inferred thermosteric contribution of ~1.2 m, this range suggests that the Greenland (7 m GMSLE) and West Antarctic (~ 5 m GMSLE) Ice Sheets were both smaller during the Mid-Pliocene, with loss of marine-based sectors of the East Antarctic Ice Sheet also possible in the case of high-end GMSL values. Note, however, that the relative contribution of these different ice sheets—and the degree to which they are in or out of phase with one another—is mainly inferred from numerical modeling studies (e.g., de Boer et al., 2017) since available observational evidence (mainly ice-rafted debris records and cosmogenic nuclide exposure ages) has coarse spatiotemporal resolution (e.g., Bierman et al., 2016).

Last Interglacial

The LIG, also referred to as the Eemian or Marine Isotope Stage 5e (MIS 5e), lasted approximately 13 thousand years from ~129 to 116 thousand years before present. Although atmospheric CO_2 concentrations are estimated to have been significantly lower than present-day values (265–285 ppm, comparable to the preindustrial era), globally averaged temperatures are thought to have been the same or higher (i.e., ~1°C above preindustrial levels; Rae et al., 2021). Moreover, due to greater orbital eccentricity during this period, polar temperatures are thought to have been significantly higher than present, with Greenland and Antarctica reaching 5°C–8°C and 3°C–5°C above preindustrial temperatures, respectively (e.g., Landais et al., 2016). GMSL estimates for this period therefore represent a useful constraint on equilibrium ice volumes during periods of prolonged warmth, even if LIG orbital forcing differs from that of the modern era.

Having previously been assumed to be negligible, a consensus is emerging that dynamic topographic perturbations to LIG sea-level markers can reach up to ~±10 m (e.g., Austermann et al., 2017). While significantly smaller than Pliocene-to-Recent deflections, these vertical land motions are of comparable magnitude to the total estimated GMSL difference between the LIG and the present, and must therefore be carefully considered when interpreting RSL markers from this period. GIA-induced RSL variation during the LIG is also of similar amplitude, albeit with a distinct spatial pattern that can, at least in theory, be separated from that of dynamic topography change.

Traditional estimates of LIG GMSL from geomorphic proxies generally correct for GIA-related sea-level change, but assume an Earth viscosity structure that varies only radially. Resulting values of peak LIG GMSL range between 4 and 9 m above present, depending on the site of the corrected sea-level markers (Dutton et al., 2015; Dyer et al., 2021). A portion of this intersite discrepancy has been resolved in certain regions by accounting for three-dimensional variations in viscosity (e.g., Austermann et al., 2021). For example, studies using radial viscosity models in their GIA calculations infer an early LIG GMSL peak of 7.6±1.7 m from sea-level indicators in the Seychelles, whereas contemporaneous estimates from Western Australia yield an estimate of ~3.4±0.6 m (Dutton and Lambeck, 2012). This ~4 m discrepancy can be reduced to ~2 m by accounting for lateral variations in viscosity and lithospheric thickness in calculations of GIA-induced RSL change (Austermann et al., 2021). The remaining ~2 m mismatch may result from variations in LIG-to-present dynamic topography change between the sites (Austermann et al., 2017); however, further work is required to conclusively validate this hypothesis.

A key complication associated with inferring LIG GMSL is the large uncertainties in the two main parameters that control GIA: ice history and mantle viscosity. Even at far-field sites, the wide range of plausible GIA model inputs propagates into GMSL uncertainties of several meters when each ice history-viscosity pair in a given model ensemble is assumed to be equally likely. To address this issue, Dyer et al. (2021) recently developed a Bayesian inverse framework that weights individual predictions of

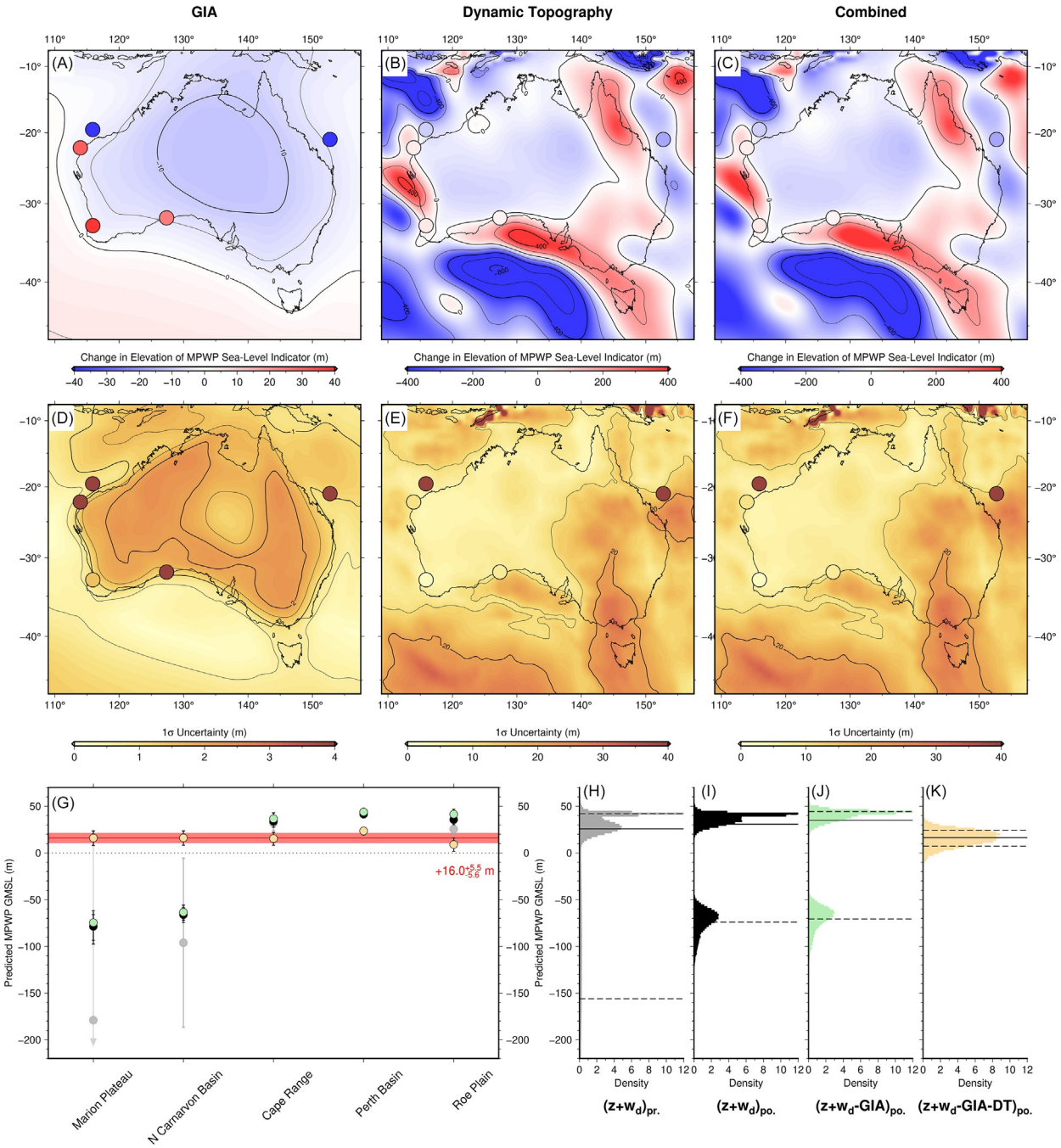

Fig. 3 Correcting Australian MPWP relative sea-level (RSL) markers for mantle dynamics. (A) GIA-induced change in MPWP sea-level marker elevation. Background color = posterior median of 3 Ma–Recent GIA-induced relative elevation change. *Circles* = prior median of uncorrected 3 Ma GMSL estimates (i.e., present-day elevation (z) + palaeo-water depth (w_d). (B) Same for dynamic topography (DT). (C) Same for combined GIA and DT contribution. (D) Uncertainty on predicted elevation change. Background color = posterior 1σ uncertainty of 3 Ma–Recent GIA-induced relative elevation change. *Circles* = prior 1σ uncertainty of uncorrected 3 Ma GMSL estimates. (E) Same for DT. (F) Same for combined GIA and DT contribution (G) DT- and GIA-corrected 3 Ma GMSL along transect anticlockwise from Marion Plateau. *Yellow circles* and *error bars* = 50th and 16th–84th percentiles of DT- and GIA-corrected posterior distribution. *Gray/black/green circles* and *error bars* = same for uncorrected prior/uncorrected posterior/GIA-corrected posterior distribution. (H) Histogram of uncorrected 3 Ma GMSL prior distribution; *solid/dashed lines* = 50th/16th–84th GMSL percentiles. (I) Same for uncorrected posterior distribution. (J) Same for GIA-corrected posterior distribution. (K) Same for DT- and GIA-corrected posterior distribution.

GIA-induced RSL change from a ~600-model ensemble based on their ability to accurately reproduce observed spatiotemporal trends in Bahamian LIG sea-level indicators (Fig. 4A–O). This approach also enables data with highly variable age and water depth uncertainties to be incorporated in a statistically robust manner. Significantly, the resulting GMSL estimate of 1.7–4.6 m (16^{th}–84^{th} percentiles) is significantly lower than most previous estimates and outside the 'likely' range of the IPCC AR6 report

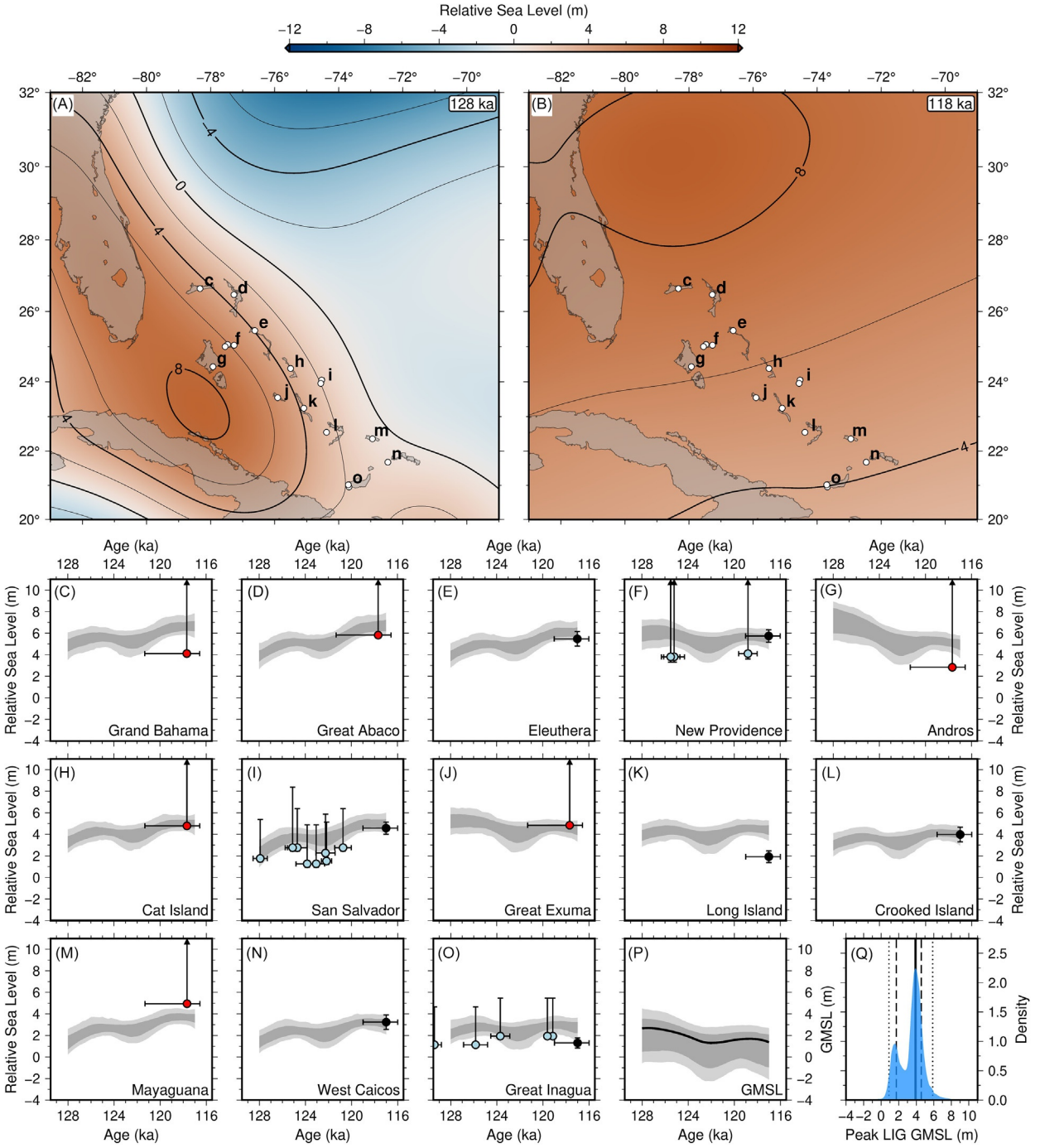

Fig. 4 Probabilistic estimation of LIG GMSL from GIA-corrected Bahamian RSL records. (A) RSL at 128 ka from maximum likelihood GIA model (assumes 96 km thick elastic lithosphere, 0.5 × 10^{21} Pa s/40 × 10^{21} Pa s upper/lower mantle viscosities, an MIS 6 Laurentide Ice Sheet containing 66 m GMSLE, and the Waelbroeck et al. (2002) GMSL curve). *White circles* = loci of LIG sea-level indicators. Labels correspond to island sites in panels C–O. (B) RSL at 118 ka. (C–O) Site-specific LIG RSL trends. *Red circles* = marine highstands; *blue circles* = corals; *black circles* = beach deposits (ordinary berms); *light/dark gray* bands = central 68%/95% of inferred posterior distribution. (P) Inferred LIG GMSL trend. *Solid line* = most likely GMSL trend (maximum *a posteriori* [MAP] probability estimate). (Q) Inferred posterior distribution of peak GMSL. *Dotted lines* = 2.5th/97.5th percentiles (0.9 m/5.9 m); *dashed lines* = 16th/84th percentiles (1.7 m/4.6 m); *solid line* = MAP estimate (3.9 m). Redrawn with permission from Dyer B, Austermann J, D'Andrea WJ, Creel RC, Sandstrom MR, Cashman M, Rovere A, and Raymo ME, (2021) Sea-level trends across the Bahamas constrain peak last interglacial ice melt. Proceedings of the National Academy of Sciences 118 (33).

(5–10 m; Fox-Kemper et al., 2021; Fig. 4P and Q). If this result is replicated elsewhere, it would imply that polar ice sheets are less sensitive to high-latitude warming than currently thought. Alternatively, if responses of the Greenland and Antarctic Ice Sheets to warming were antiphased, elevated ice sheet sensitivity would remain a possibility.

The timing of peak GMSL within the LIG is controversial with different studies arguing for an early peak, a late peak, and even multiple peaks due to orbitally driven asynchronicity in ice loss from the Antarctic and Greenland Ice Sheets (Horton et al., 2018).

Ice-sheet modeling and ice core-based reconstructions are beginning to reach consensus on a 0.5–3.5 m LIG sea-level contribution from the Greenland Ice Sheet (e.g., Plach et al., 2019), while an additional ~1 m is expected due to thermal expansion and melting of mountain glaciers (Rohling et al., 2019). The Antarctic contribution to LIG GMSL remains unclear since large uncertainties in peak LIG GMSL combined with a lack of direct evidence for contemporaneous mass loss permit values anywhere between 0 and 6 m GMSLE.

Other Plio-Pleistocene warm periods

Pliocene Climatic Optimum

The Pliocene Climatic Optimum (PCO; ~4.4–4.0 Ma) was the warmest interval in the last 5 million years, with global mean temperatures approximately 4°C higher than preindustrial values and elevated atmospheric CO_2 (~400–470 ppm; Rae et al., 2021). Geomorphic sea-level indicators from this period are sparse, complicating assessment of GMSL. However, records from Mallorca and Argentina that have been locally corrected for long-term uplift and GIA indicate a GMSL of 11–28 m (Dumitru et al., 2019; Hollyday et al., 2023), broadly consistent with ice-sheet modeling studies that suggest ~8.5 m and ~7 m GMSLE contributions from Antarctica and Greenland, respectively, with an additional ~1.5 m from thermosteric effects (Golledge et al., 2017). A >4 m Antarctic contribution is compatible with independent evidence from offshore sedimentary records, which suggest significant early Pliocene ice loss in the Wilkes Subglacial Basin of East Antarctica (Bertram et al., 2018). Similarly, the limited volume of ice rafted debris recorded offshore Greenland implies only small, ephemeral ice sheets were present during this interval (Bailey et al., 2013). Consensus therefore appears to be building that the PCO was characterized by lower ice volume and higher GMSL than the MPWP, consistent with its more elevated CO_2 and temperature levels. It may therefore provide a useful guide to future sea-level trajectories in the event that atmospheric CO_2 remains significantly above 400 ppm throughout the coming centuries.

MIS 11

MIS 11 (~420–370 ka) was a peculiarly long interglacial and details of the climatic conditions during this period remain somewhat enigmatic. Global mean temperature estimates range from 1°C to 2°C above preindustrial levels and atmospheric CO_2 concentrations appear to have been similar to other Quaternary interglacials (~280 ppm; Rae et al., 2021). However, sea-level reconstructions that have been corrected for tectonic deformation and GIA indicate a remarkably large reduction in polar ice volumes (6–13 m GMSLE) during this period, an inference corroborated by independent geochemical and palaeobiological datasets that point to substantial retreat of both the Antarctic and Greenland ice sheets (Roberts et al., 2012; Raymo and Mitrovica, 2012; Tzedakis et al., 2022). The unusually protracted duration of this interglacial was likely key to triggering such widespread ice loss, and has been linked to antiphasing of obliquity and precession cycles (Tzedakis et al., 2022). These atypical features complicate direct comparisons of MIS 11 with ongoing climatic changes.

MIS 11 palaeoshorelines from relatively tectonically stable regions are restricted to single sites in the Bahamas, Bermuda, eastern USA, southeastern Australia, and South Africa. This sparse spatial distribution hinders efforts to deconvolve RSL changes induced by GIA and dynamic topography from GMSL variations during this period, leading to deep uncertainty in existing sea-level estimates. An additional complication is that ice histories are not well constrained in the lead-up to MIS 11, limiting the precision and accuracy of GIA predictions across this interval (Tzedakis et al., 2022). Nevertheless, the balance of current evidence suggests that MIS 11 GMSL had a higher peak than the LIG, with substantial loss of ice from southern Greenland and the Wilkes Basin in East Antarctica.

Mid-Holocene Warm Period

Proxy records suggest that the Mid-Holocene Warm Period (MHWP; ~8–3 ka) was characterized by marginally lower global mean temperature (~ 0.75°C above preindustrial levels) and atmospheric CO_2 (260–270 ppm) than the LIG, although Northern Hemisphere temperatures may have reached ~4°C above preindustrial levels (Dutton et al., 2015; Rae et al., 2021). However, the proposed long-term cooling trend following this early peak is at odds with climate simulations that point to progressive warming over the same time interval (Horton et al., 2018). This discrepancy is yet to be resolved, confounding efforts to understand the mechanisms driving climatic changes throughout this period. Nevertheless, sea-level evolution over the MHWP is relatively well constrained thanks to an abundance of preserved coastal deposits and the applicability of high-resolution dating techniques. In addition, the recency of this warm period minimizes pollution of the GMSL signal with dynamic topography and enables accurate reconstruction of past ice extent (at least in the Northern Hemisphere), allowing spatial variations in RSL to be more confidently tied to GIA processes.

Far-field GMSL estimates during this period obtain a peak of 1–6 m (Horton et al., 2018). Much of this apparent highstand is attributed to equatorial ocean siphoning; however, some evidence exists for a less extensive West Antarctic Ice Sheet at this time (Kingslake et al., 2018). If readvance of this ice sheet following the Mid-Holocene is proven, it would underline how local GIA-induced changes in bedrock elevation can interact with global scale sea-level changes, partially decoupling GMSL variation from coeval climatic changes. Despite this uncertainty in mid-Holocene Antarctic ice volumes, this period provides important constraints on the typical rate of interglacial sea-level change resulting from natural climate variability, allowing the recent acceleration in GMSL rise to be confidently attributed to anthropogenic impacts.

Summary

Increasingly accurate correction of RSL data for post-depositional geodynamic perturbations is yielding new insight into ice volumes during past warm periods. These analyses generally reduce inferred palaeo-GMSL for key warm periods, bringing them into better agreement with predictions from ice-sheet modeling studies. It therefore appears, perhaps unsurprisingly, that a significant fraction of the pre-existing discrepancy resulted from a bias in the palaeoshoreline record toward regions experiencing long-term RSL fall.

Revised palaeo-GMSL estimates correlate strongly with contemporaneous global mean temperature reconstructions, although this relationship is clearly nonlinear (Fig. 5). An additional complication is that the timescale over which warming is sustained may exert a strong control on palaeo-ice volume (e.g., compare sea-levels during MIS 5e and MIS 11). Overall, constraint on peak GMSL during key warm periods has improved significantly in the past decade. However, determining the relative contribution of Greenland, West Antarctica, and East Antarctica to past sea-level change remains challenging due to the current sparsity of palaeoshoreline data and direct constraints on former ice extents. In addition, it is unclear how mantle flow-driven changes in bed elevations may have altered the equilibrium grounded ice capacity of these ice sheets through time. Resolving these issues is crucial for ongoing efforts to better integrate palaeo sea-level constraints into future sea-level projections.

Outlook: Refining sea-level reconstructions with new datasets and geodynamic modeling techniques

Significant improvements in intermediate and long-term projections of future sea-level rise can be achieved if uncertainty on palaeo sea levels can be narrowed and revised estimates can be better integrated into modeling studies. Three key challenges currently

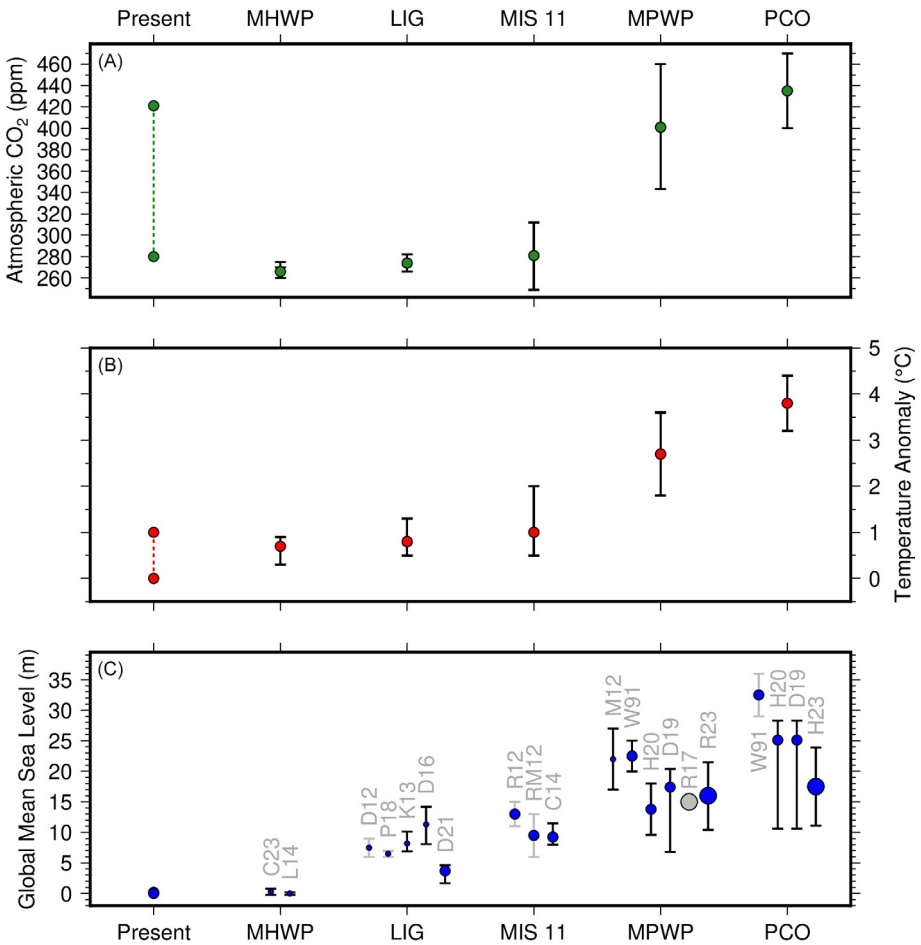

Fig. 5 Summary of climatic variables during key warm periods. (A) Atmospheric CO_2 (Brovkin et al., 2016; Rae et al., 2021). *Dotted lines* connect between preindustrial and present-day conditions. (B) mean global surface temperature (Burke et al., 2018; Rachmayani et al., 2017; Tzedakis et al., 2022; Brierley and Fedorov, 2010). (C) GMSL. *Gray symbol/blue* with *gray error bar/blue* with *black error bar* = no/limited/comprehensive uncertainty quantification; *small/medium/large symbol* = uncorrected/indirectly corrected/directly corrected for dynamic topography-induced RSL changes. C23 = (Creel et al., 2022); L14 = (Lambeck et al., 2014); D12 = (Dutton and Lambeck, 2012); P18 = (Polyak et al., 2018); K13 = (Kopp et al., 2013); D16 = (Düsterhus et al., 2016); D21 = (Dyer et al., 2021); R12 = (Roberts et al., 2012); RM12 = (Raymo and Mitrovica, 2012); C14 = (Chen et al., 2014); M12 = (Miller and Becker, 2012); W91 = (Wardlaw and Quinn, 1991); H20 = (Hearty et al., 2020); D19 = (Dumitru et al., 2019); R17 = (Moucha and Ruetenik, 2017); R23 = (Richards et al., 2022); H23 = (Hollyday et al., 2023).

impede efforts to increase precision and accuracy of GMSL estimates during past warm periods. First, the sparsity of existing geomorphic sea-level constraints complicates the differentiation of GMSL changes from spatially variable RSL signals related to post-depositional geodynamic processes. Secondly, the accuracy with which these RSL changes can be constrained, especially those arising from GIA and dynamic topography, is limited by uncertain mantle viscosity and density structure. The following sections outline possible solutions to each of these challenges.

Improving palaeo-sea level data coverage

Natural limits on the formation and preservation of palaeoshoreline deposits place an upper bound on achievable data densities, which becomes more restrictive as the age of the targeted sea-level highstand increases. Nevertheless, significant gaps in the Neogene sea-level record can be filled by leveraging existing data compilations. For example, the PalaeoDB palaeobiological database contains global information on the occurrence of shallow marine fauna that—despite generally having larger uncertainties than data from more targeted field studies—allow GIA and dynamic topography predictions to be groundtruthed (Fernandes and Roberts, 2021). Similarly, the abundance of publicly available well and seismic reflection datasets is constantly increasing thanks to data sharing agreements between governmental organizations (e.g., Geoscience Australia) and the geoenergy industry, allowing backstripping techniques to be applied to a significant fraction of the world's continental margins. Although uncertainties associated with sediment compaction diminish the precision of backstripped sea-level records, their relative temporal continuity allows local RSL trends to be inferred with reasonable reliability. Finally, continental-scale hiatus maps, derived from analysis of conformable and unconformable contacts between rocks from successive geological series, are sufficiently spatially complete to provide useful validation of geodynamic model predictions despite their coarse temporal resolution (Hayek et al., 2020).

Continuous improvements in dating and data acquisition techniques are constantly increasing the spatio-temporal resolution of the global palaeo-sea level record. Community efforts to build new sea-level databases with standardized entry formats represent a particularly important advance, for example, the WALIS (World Atlas of Last Interglacial Shorelines) project (Rovere et al., 2022). Machine learning techniques are also showing significant promise as a tool for expanding data coverage, with neural networks increasingly used to automate detection of shallow marine facies in satellite-derived digital elevation models (e.g., Dyer et al., 2021). In addition, integration of GIA and dynamic topography model predictions within probabilistic inverse frameworks can guide the sampling strategy of new field campaigns by quantifying the extent to which additional data points in a given region will reduce uncertainty in sea-level reconstructions. Finally, innovative dating techniques, such as multiple-isotope cosmogenic nuclide approaches, coupled with continued improvement in the precision of long-established methods, will enable the identification of new Plio-Pleistocene shorelines and improve age constraint on existing deposits.

Improving models of post-depositional impacts

In recent decades, our ability to numerically model the impact of GIA and dynamic topography on RSL indicators has grown significantly. However, it has also become increasingly apparent that more accurate constraints on the 3D variations in mantle viscosity and density that drive these processes are urgently needed. Fortunately, a number of recent breakthroughs indicate that meeting this requirement is possible, at least regionally. First, new data compilations that constrain present-day dynamic topography—when combined with existing non-hydrostatic geoid height anomaly and core-mantle boundary excess ellipticity measurements—have allowed Earth's internal density and viscosity structure to be quantified in greater detail (Lu et al., 2020; Richards et al., 2023). Second, theoretical and computational advances in seismic tomography are enabling higher resolution imaging of Earth's internal structure. Improved constraint on velocity variations within the lithosphere and asthenosphere is especially valuable since GIA and dynamic topography signals are dominated by shallow mantle structure on Plio-Pleistocene timescales. Third, experimental constraints on the elastic and anelastic behavior of rocks at seismic frequencies are improving our ability to convert Earth's present-day seismic velocity structure into the physical quantities of interest for GIA and dynamic topography modeling (i.e., temperature, density, and viscosity; Austermann et al., 2021; Lau et al., 2021; Ivins et al., 2023; Hazzard et al., 2023). Finally, powerful adjoint-based inverse methods have been developed that enable reliable reconstruction of mantle flow back through time ('retrodiction') and allow inferred three-dimensional viscosity structure to be refined using RSL observations ('viscosity tomography'; Ghelichkhan and Bunge, 2018; Crawford et al., 2018).

Despite these innovations, the computational expense of calculating time-dependent changes in GIA and dynamic topography using Earth models that include three-dimensional variations in physical properties is substantial. In addition, although constraint on present-day Earth structure has improved, significant uncertainty remains due to limits on tomographic resolution and nonunique conversions between seismic velocity and key physical properties. Given these twin difficulties, accurately propagating uncertainties in Earth structure into GMSL estimates is currently problematic. However, new techniques that enable rapid calculation of approximate solutions (e.g., statistical emulation and surrogate modeling) may partially resolve these problems by unlocking the ability to integrate complex model calculations into a probabilistic inverse framework. Some of these frameworks also allow the incorporation of data with very different age uncertainties and palaeo-water depth ranges. These advances are critical since improving the sea-level projections of ice-sheet models will rely on robust assessments of palaeo-GMSL that rigorously account for all these sources of uncertainty.

Synthesis

Over the past decades, it has become increasingly clear that a broad range of geodynamic phenomena can cause RSL to deviate significantly from globally averaged values (GMSL). The characteristic timescales, wavelengths, and spatial patterns of these sea-level perturbations vary significantly depending on the underlying process. Mantle dynamic topography evolves slowest ($\sim$0.1 mm year^{-1}) but has a ubiquitous impact and can produce hundred-meter deflections in a few million years. By contrast, tectonic activity can produce meter-scale elevation changes on centennial timescales, but such extreme vertical displacement is largely confined to narrow regions along convergent plate boundaries. This separation of scales, patterns, and magnitudes suggests that, with sufficient data coverage and continued improvement in our understanding of the solid Earth, RSL patterns associated with different mechanisms can be detected, quantified, and corrected for, at least locally.

Although post-depositional geodynamic processes undoubtedly complicate the assessment of palaeo-GMSL, significant progress has been made thanks to new RSL data, improved constraint on Earth's internal structure, and advances in geodynamic and probabilistic modeling. Consensus is now building that GMSL during the MPWP did not exceed $\sim$22 m. This upper bound suggests that, if the Greenland Ice Sheet was less extensive than at the present-day, a significant fraction of East Antarctic marine-based ice must have persisted during this period. Similarly, recent correction of LIG sea levels for mantle dynamic topography and GIA produces an upper limit (84th percentile) on peak GMSL of $\sim$4 m, lower than many previous estimates (6–9 m). If confirmed, these reductions imply that some existing ice-sheet-model-based sea-level projections need to be revised downwards as they are calibrated against LIG and MPWP GMSL bounds that are excessively high.

It is clear from Holocene records that present rates of sea-level change are significantly more rapid than at any other time during the present interglacial. However, longer term trajectories remain unclear due, in large part, to remaining uncertainties in the palaeo sea-level record. Significant progress can be made by increasing data coverage during poorly sampled intervals (e.g., the PCO and MIS 11) as well as corroborating recent low-end MPWP and LIG sea-level estimates in other regions. These goals are increasingly achievable thanks to recent improvements in data availability, advances in our knowledge of solid Earth structure and dynamics, and the development of Bayesian frameworks to rigorously propagate uncertainties in both geodynamic model parameters and sea-level data into inferred GMSL histories. These probabilistic frameworks also allow the main sources of uncertainty to be identified, enabling field data collection and model refinement to be better targeted. Connecting palaeo sea-level variation to present and near-future trends will remain challenging due to inherent uncertainties and evolving climatic boundary conditions. Nevertheless, recent breakthroughs in palaeo sea-level reconstruction have enabled uncertainty in future projections to be both narrowed and robustly quantified in a manner that was previously infeasible.

References

Austermann J, Pollard D, Mitrovica JX, Moucha R, Forte AM, DeConto RM, Rowley DB, and Raymo ME (2015) The impact of dynamic topography change on Antarctic ice sheet stability during the mid-Pliocene warm period. *Geology* 43(10): 927–930.

Austermann J, Mitrovica JX, Huybers P, and Rovere A (2017) Detection of a dynamic topography signal in last interglacial sea-level records. *Science Advances* 3(7): e1700457.

Austermann J, Hoggard MJ, Latychev K, Richards FD, and Mitrovica JX (2021) The effect of lateral variations in Earth structure on last interglacial sea level. *Geophysical Journal International* 227: 1938–1960.

Bailey I, Hole GM, Foster GL, Wilson PA, Storey CD, Trueman CN, and Raymo ME (2013) An alternative suggestion for the Pliocene onset of major northern hemisphere glaciation based on the geochemical provenance of North Atlantic Ocean ice-rafted debris. *Quaternary Science Reviews* 75: 181–194.

Barletta VR, Bevis M, Smith BE, Wilson T, Brown A, Bordoni A, Willis M, Khan SA, Rovira-Navarro M, Dalziel I, et al. (2018) Observed rapid bedrock uplift in Amundsen sea embayment promotes ice-sheet stability. *Science* 360(6395): 1335–1339.

Bertram RA, Wilson DJ, van de Flierdt T, McKay RM, Patterson MO, Jimenez-Espejo FJ, Escutia C, Duke GC, Taylor-Silva BI, and Riesselman CR (2018) Pliocene deglacial event timelines and the biogeochemical response offshore Wilkes subglacial basin, East Antarctica. *Earth and Planetary Science Letters* 494: 109–116.

Bierman PR, Shakun JD, Corbett LB, Zimmerman SR, and Rood DH (2016) A persistent and dynamic East Greenland ice sheet over the past 7.5 million years. *Nature* 540(7632): 256–260.

Brierley CM and Fedorov AV (2010) Relative importance of meridional and zonal sea surface temperature gradients for the onset of the ice ages and Pliocene-Pleistocene climate evolution. *Paleoceanography* 25(2): PA2214.

Brovkin V, Brücher T, Kleinen T, Zaehle S, Joos F, Roth R, Spahni R, Schmitt J, Fischer H, Leuenberger M, et al. (2016) Comparative carbon cycle dynamics of the present and last interglacial. *Quaternary Science Reviews* 137: 15–32.

Bungum H and Eldholm O (2022) The conundrums of the postglacial tectonic response of the Fennoscandian and Canadian shields. *Earth-Science Reviews* 232: 104146.

Burbidge DR, Gesto FN, Kohn BP, and Cummins PR (2009) Constraints on the current rate of deformation and surface uplift of the Australian continent from a new seismic database and low-T thermochronological data. *Australian Journal of Earth Sciences* 56(2): 99–110.

Burke KD, Williams JW, Chandler MA, Haywood AM, Lunt DJ, and Otto-Bliesner BL (2018) Pliocene and Eocene provide best analogs for near-future climates. *Proceedings of the National Academy of Sciences* 115(52): 13288–13293.

Chen F, Friedman S, Gertler CG, Looney J, O'Connell N, Sierks K, and Mitrovica JX (2014) Refining estimates of polar ice volumes during the MIS11 interglacial using sea level records from South Africa. *Journal of Climate* 27(23): 8740–8746.

Conrad C and Husson L (2009) Influence of dynamic topography on sea level and its rate of change. *Lithosphere* 1: 110–120. https://doi.org/10.1130/L32.1.

Crawford O, Al-Attar D, Tromp J, Mitrovica JX, Austermann J, and Lau HCP (2018) Quantifying the sensitivity of post-glacial sea level change to laterally varying viscosity. *Geophysical Journal International* 214(2): 1324–1363.

Creel R, Austermann J, Kopp R, Khan N, Ashe E, Kingslake J, and Albrecht T (2022) Probabilistic estimation of mid-Holocene global mean sea level. In: *EGU General Assembly Conference Abstracts*. EGU22–1953.

Creveling JR, Austermann J, and Dutton A (2019) Uplift of trail ridge, Florida, by karst dissolution, glacial isostatic adjustment, and dynamic topography. *Journal of Geophysical Research: Solid Earth* 124(12): 13354–13366.

Dalton CA, Wilson DS, and Herbert TD (2022) Evidence for a global slowdown in seafloor spreading since 15 Ma. *Geophysical Research Letters* 49(6). e2022GL097937.
de Boer B, Haywood AM, Dolan AM, Hunter SJ, and Prescott CL (2017) The transient response of ice volume to orbital forcing during the warm late pliocene. *Geophysical Research Letters* 44(20): 10–486.
Dumitru OA, Austermann J, Polyak VJ, Fornós JJ, Asmerom Y, Ginés J, Ginés A, and Onac BP (2019) Constraints on global mean sea level during Pliocene warmth. *Nature* 574(7777): 233–236.
Düsterhus A, Tamisiea ME, and Jevrejeva S (2016) Estimating the sea level highstand during the last interglacial: A probabilistic massive ensemble approach. *Geophysical Journal International* 206(2): 900–920.
Dutton A and Lambeck K (2012) Ice volume and sea level during the last interglacial. *Science* 337(6091): 216–219.
Dutton A, Carlson AE, Long A, Milne GA, Clark PU, DeConto R, Horton BP, Rahmstorf S, and Raymo ME (2015) Sea-level rise due to polar ice-sheet mass loss during past warm periods. *Science* 349(6244): aaa4019.
Dyer B, Austermann J, D'Andrea WJ, Creel RC, Sandstrom MR, Cashman M, Rovere A, and Raymo ME (2021) Sea-level trends across the Bahamas constrain peak last interglacial ice melt. *Proceedings of the National Academy of Sciences* 118(33): e2026839118.
Fernandes VM and Roberts GG (2021) Cretaceous to recent net continental uplift from paleobiological data: Insights into sub-plate support. *Bulletin* 133(5–6): 1217–1236.
Forte AM and Rowley DB (2022) Earth's isostatic and dynamic topography—A critical perspective. *Geochemistry, Geophysics, Geosystems* 23(9). e2021GC009740.
Fox-Kemper B, Hewitt HT, Xiao C, Aðalgeirsdóttir G, Drijfhout SS, Edwards TL, Golledge NR, Hemer M, Kopp RE, Krinner G, Mix A, Notz D, Nowicki S, Nurhati IS, Ruiz L, Sallée J-B, Slangen ABA, and Yu Y (2021) Ocean, cryosphere and sea level change. In: Masson-Delmotte V, Zhai P, Pirani A, Connors SL, Péan C, Berger S, et al. (eds.) *Climate Change 2021: The Physical Science Basis. Contribution of Working Group I to the Sixth Assessment Report of the Intergovernmental Panel on Climate Change*, pp. 1211–1362. Cambridge and New York, NY: Cambridge University Press.
Ghelichkhan S and Bunge H-P (2018) The adjoint equations for thermochemical compressible mantle convection: Derivation and verification by twin experiments. *Proceedings of the Royal Society A: Mathematical, Physical and Engineering Sciences* 474(2220): 20180329.
Golledge NR, Thomas ZA, Levy RH, Gasson EGW, Naish TR, McKay RM, Kowalewski DE, and Fogwill CJ (2017) Antarctic climate and ice-sheet configuration during the early Pliocene interglacial at 4.23 Ma. *Climate of the Past* 13(7): 959–975.
Grant GR and Naish TR (2021) Pliocene sea level revisited: Is there more than meets the eye? *Past Global Changes Magazine* 29(1): 34–35.
Hayek JN, Vilacís B, Bunge H-P, Friedrich AM, Carena S, and Vibe Y (2020) Continent-scale Hiatus maps for the Atlantic realm and Australia since the upper jurassic and links to mantle flow induced dynamic topography. *Proceedings of the Royal Society A: Mathematical, Physical and Engineering Sciences* 476(2242): 20200390. https://doi.org/10.1098/rspa.2020.0390.
Hazzard JAN, Richards FD, Goes SDB, and Roberts GG (2023) Probabilistic assessment of Antarctic thermomechanical structure: Impacts on ice sheet stability. *Journal of Geophysical Research: Solid Earth* 128(5): e2023JB026653. https://doi.org/10.1029/2023JB026653.
Hearty PJ, Rovere A, Sandstrom MR, O'Leary MJ, Roberts D, and Raymo ME (2020) Pliocene-Pleistocene stratigraphy and sea-level estimates, Republic of South Africa with implications for a 400 ppmv CO2 world. *Paleoceanography and Paleoclimatology* 35(7). e2019PA003835.
Hibbert FD, Rohling EJ, Dutton A, Williams FH, Chutcharavan PM, Zhao C, and Tamisiea ME (2016) Coral indicators of past sea-level change: A global repository of U-series dated benchmarks. *Quaternary Science Reviews* 145: 1–56.
Hoggard M, Austermann J, Randel C, and Stephenson S (2021) Observational estimates of dynamic topography through space and time. In: *Mantle Convection and Surface Expressions*, pp. 371–411. American Geophysical Union (AGU).
Hollyday A, Austermann J, Lloyd A, Hoggard M, Richards F, and Rovere A (2023) A revised estimate of early Pliocene global mean sea level using geodynamic models of the Patagonian slab window. *Geochemistry, Geophysics, Geosystems* 24: e2022GC010648.
Horton BP, Kopp RE, Garner AJ, Hay CC, Khan NS, Roy K, and Shaw TA (2018) Mapping sea-level change in time, space, and probability. *Annual Review of Environment and Resources* 43: 481–521.
Huppert KL, Royden LH, and Perron JT (2015) Dominant influence of volcanic loading on vertical motions of the Hawaiian Islands. *Earth and Planetary Science Letters* 418: 149–171.
Ivins ER, van der Wal W, Wiens DA, Lloyd AJ, and Caron L (2023) Antarctic upper mantle rheology. *Geological Society, London, Memoirs* 56(1): 267–294.
Kingslake J, Scherer RP, Albrecht T, Coenen J, Powell RD, Reese R, Stansell ND, Tulaczyk S, Wearing MG, and Whitehouse PL (2018) Extensive retreat and re-advance of the West Antarctic ice sheet during the Holocene. *Nature* 558(7710): 430–434.
Kopp RE, Simons FJ, Mitrovica JX, Maloof AC, and Oppenheimer M (2013) A probabilistic assessment of sea level variations within the last interglacial stage. *Geophysical Journal International* 193(2): 711–716.
Kopp RE, Hay CC, Little CM, and Mitrovica JX (2015) Geographic variability of sea-level change. *Current Climate Change Reports* 1: 192–204.
Lambeck K, Rouby H, Purcell A, Sun Y, and Sambridge M (2014) Sea level and global ice volumes from the last glacial maximum to the Holocene. *Proceedings of the National Academy of Sciences* 111(43): 15296–15303.
Landais A, Masson-Delmotte V, Capron E, Langebroek PM, Bakker P, Stone EJ, Merz N, Raible CC, Fischer H, Orsi A, et al. (2016) How warm was Greenland during the last interglacial period? *Climate of the Past* 12(9): 1933–1948.
Lau HCP, Austermann J, Holtzman BK, Havlin C, Lloyd AJ, Book C, and Hopper E (2021) Frequency dependent mantle viscoelasticity via the complex viscosity: Cases from Antarctica. *Journal of Geophysical Research: Solid Earth* 126(11): e2021JB022622.
Lu C, Forte AM, Simmons NA, Grand SP, Kajan MN, Lai H, and Garnero EJ (2020) The sensitivity of joint inversions of seismic and geodynamic data to mantle viscosity. *Geochemistry, Geophysics, Geosystems* 21(4): e2019GC008648.
Malatesta LC, Finnegan NJ, Huppert KL, and Carre no EI (2022) The influence of rock uplift rate on the formation and preservation of individual marine terraces during multiple sea-level stands. *Geology* 50(1): 101–105.
Miller MS and Becker TW (2012) Mantle flow deflected by interactions between subducted slabs and cratonic keels. *Nature Geoscience* 5: 726–730. https://doi.org/10.1038/ngeo1553.
Miller KG, Browning JV, Schmelz WJ, Kopp RE, Mountain GS, and Wright JD (2020) Cenozoic sea-level and cryospheric evolution from deep-sea geochemical and continental margin records. *Science Advances* 6(20): eaaz1346.
Mitrovica JX and Milne GA (2002) On the origin of late Holocene sea-level highstands within equatorial ocean basins. *Quaternary Science Reviews* 21(20-22): 2179–2190.
Mitrovica JX, Wahr J, Matsuyama I, and Paulson A (2005) The rotational stability of an ice-age Earth. *Geophysical Journal International* 161(2): 491–506.
Moucha R and Ruetenik GA (2017) Interplay between dynamic topography and flexure along the US Atlantic passive margin: Insights from landscape evolution modeling. *Global and Planetary Change* 149: 72–78.
Müller RD, Sdrolias M, Gaina C, and Roest WR (2008) Age, spreading rates and spreading asymmetry of the world's ocean crust. *Geochemistry, Geophysics, Geosystems* 9: Q04006.
Murray-Wallace CV and Woodroffe CD (2014) *Quaternary Sea-Level Changes: A Global Perspective*. Cambridge University Press.
Pfeffer J, Spada G, Mémin A, Boy J-P, and Allemand P (2017) Decoding the origins of vertical land motions observed today at coasts. *Geophysical Journal International* 210(1): 148–165.
Pico T (2020) Towards assessing the influence of sediment loading on last interglacial sea level. *Geophysical Journal International* 220(1): 384–392.
Plach A, Nisancioglu KH, Langebroek PM, Born A, et al. (2019) Eemian Greenland ice sheet simulated with a higher-order model shows strong sensitivity to surface mass balance forcing. *The Cryosphere* 13(8): 2133–2148.
Polyak VJ, Onac BP, Fornós JJ, Hay C, Asmerom Y, Dorale JA, Ginés J, Tuccimei P, and Ginés A (2018) A highly resolved record of relative sea level in the Western Mediterranean sea during the last interglacial period. *Nature Geoscience* 11(11): 860–864.

Rachmayani R, Prange M, Lunt DJ, Stone EJ, and Schulz M (2017) Sensitivity of the Greenland ice sheet to interglacial climate forcing: MIS 5e versus MIS 11. *Paleoceanography* 32(11): 1089–1101.

Rae JWB, Zhang YG, Liu X, Foster GL, Stoll HM, and Whiteford RDM (2021) Atmospheric CO2 over the past 66 million years from marine archives. *Annual Review of Earth and Planetary Sciences* 49: 609–641.

Ramalho RS, Helffrich G, Madeira J, Cosca M, Thomas C, Quartau R, Hipólito A, Rovere A, Hearty PJ, and Ávila SP (2017) Emergence and evolution of Santa Maria Island (Azores)—The conundrum of uplifted islands revisited. *GSA Bulletin* 129(3–4): 372–390.

Raymo ME (1994) The initiation of northern hemisphere glaciation. *Annual Review of Earth and Planetary Sciences* 22(1): 353–383.

Raymo ME and Mitrovica JX (2012) Collapse of polar ice sheets during the stage 11 interglacial. *Nature* 483(7390): 453–456.

Raymo ME, Mitrovica JX, O'Leary MJ, DeConto RM, and Hearty PJ (2011) Departures from eustasy in Pliocene sea-level records. *Nature Geoscience* 4(5): 328–332.

Raymo ME, Kozdon R, Evans D, Lisiecki L, and Ford HL (2018) The accuracy of mid-Pliocene δ^{18}O-based ice volume and sea level reconstructions. *Earth-Science Reviews* 177: 291–302.

Richards FD, Coulson S, Hoggard M, Austermann J, Dyer B, and Mitrovica JX (2022) Correcting for mantle dynamics reconciles mid-Pliocene sea-level estimates. *EarthArXiv*.

Richards FD, Hoggard MJ, Ghelichkhan S, Koelemeijer P, and Lau HCP (2023) Geodynamic, geodetic, and seismic constraints favour deflated and dense-cored LLVPs. *Earth and Planetary Science Letters* 602: 117964.

Roberts DL, Karkanas P, Jacobs Z, Marean CW, and Roberts RG (2012) Melting ice sheets 400,000 yr ago raised sea level by 13 m: Past analogue for future trends. *Earth and Planetary Science Letters* 357: 226–237.

Rohling EJ, Hibbert FD, Grant KM, Galaasen EV, Irvalı N, Kleiven HF, Marino G, Ninnemann U, Roberts AP, Rosenthal Y, et al. (2019) Asynchronous Antarctic and Greenland ice-volume contributions to the last interglacial sea-level highstand. *Nature Communications* 10(1): 5040.

Rovere A, Ryan DD, Vacchi M, Dutton A, Simms AR, and Murray-Wallace CV (2022) The world atlas of last interglacial shorelines (version 1.0). *Earth System Science Data Discussions* 15: 1–37.

Tzedakis PC, Hodell DA, Nehrbass-Ahles C, Mitsui T, and Wolff EW (2022) Marine isotope stage 11c: An unusual interglacial. *Quaternary Science Reviews* 284: 107493.

Waelbroeck C, Labeyrie L, Michel E, Duplessy J-C, Mcmanus JF, Lambeck K, Balbon E, and Labracherie M (2002) Sea-level and deep water temperature changes derived from benthic foraminifera isotopic records. *Quaternary Science Reviews* 21(1–3): 295–305.

Wardlaw BR and Quinn TM (1991) The record of Pliocene sea-level change at Enewetak Atoll. *Quaternary Science Reviews* 10(2–3): 247–258.

Watts AB (2001) *Isostasy and Flexure of the Lithosphere*. Cambridge University Press.

Wright NM, Seton M, Williams SE, Whittaker JM, and Müller RD (2020) Sea-level fluctuations driven by changes in global ocean basin volume following supercontinent break-up. *Earth-Science Reviews* 208: 103293.

Young A, Flament N, Hall L, and Merdith A (2021) The influence of mantle flow on intracontinental basins: Three examples from Australia. *Basin Research* 33: 1429–1453.

Young A, Flament N, Williams SE, Merdith A, Cao X, and Müller RD (2022) Long-term phanerozoic sea level change from solid Earth processes. *Earth and Planetary Science Letters* 584: 117451.